# The time-programmable frequency comb and its use in quantum-limited ranging

https://doi.org/10.1038/s41586-022-05225-8

Emily D. Caldwell<sup>1,2</sup>, Laura C. Sinclair<sup>1⊠</sup>, Nathan R. Newbury<sup>1⊠</sup> & Jean-Daniel Deschenes<sup>3</sup>

Received: 16 April 2022

Accepted: 11 August 2022

Published online: 5 October 2022



Check for updates

Two decades after its invention, the classic self-referenced frequency comb laser is an unrivalled ruler for frequency, time and distance metrology owing to the rigid spacing of its optical output<sup>1,2</sup>. As a consequence, it is now used in numerous sensing applications that require a combination of high bandwidth and high precision<sup>3-5</sup>. Many of these applications, however, are limited by the trade-offs inherent in the rigidity of the comb output and operate far from quantum-limited sensitivity. Here we demonstrate an agile programmable frequency comb where the pulse time and phase are digitally controlled with ±2-attosecond accuracy. This agility enables quantum-limited sensitivity in sensing applications as the programmable comb can be configured to coherently track weak returning pulse trains at the shot-noise limit. To highlight its capabilities, we use this programmable comb in a ranging system, reducing the required power to reach a given precision by about 5,000-fold compared with a conventional dual-comb system. This enables ranging at a mean photon per pulse number of 1/77 while retaining the full accuracy and precision of a rigid frequency comb. Beyond ranging and imaging 6-12. applications in time and frequency metrology<sup>1,2,5,13-23</sup>, comb-based spectroscopy<sup>24-32</sup>,  $pump-probe\ experiments^{33}\ and\ compressive\ sensing^{34,35}\ should\ benefit\ from\ coherent$ control of the comb-pulse time and phase.

As applications of frequency combs have expanded, their uses have extended beyond functioning simply as a reference ruler<sup>3-5</sup>. For example, many experiments combine two or more frequency combs for active sensing, including precision ranging and imaging<sup>6-12</sup>, linear and nonlinear spectroscopy $^{24-32}$ , and time transfer $^{13-20,23}$ . In these applications, the multiple fixed combs serve as differential rulers by phase-locking them to have a vernier-like offset between their frequency comb lines, or their pulses in time. Although these applications exploit the accuracy and precision of frequency combs, they operate nowhere near the quantum (or shot noise) limit, despite the use of heterodyne detection, because of effective dead time owing to sensing the incoming signal-comb light via a comb with a deliberately mismatched repetition frequency. Consequently, there are strong trade-offs in measurement speed, sensitivity and resolution<sup>24,36,37</sup>. In some dual-comb ranging and spectroscopy demonstrations, these penalties have been partially addressed by incoherent modulation of the comb<sup>38-41</sup> but not eliminated.

Here we overlay a self-referenced optical frequency comb with synchronous digital electronics for real-time coherent control of the comb's pulse train output. We manipulate the frequency comb's two phase locks to dynamically control and track the time and phase of the frequency comb's output pulses at will. The temporal placement of the comb pulses is set with ±2-attosecond (as) accuracy with a range  $limited \ only \ by \ slew-rate \ considerations. \ This \ time-programmable$ frequency comb (TPFC) goes beyond the 'mechanical gear box' analogy often applied to optically self-referenced combs<sup>5</sup>, replacing it with a digitally controllable, agile, coherent optical pulse source. The agility of the TPFC enables many more measurement modalities than a rigid frequency comb. In sensing applications, the TPFC can enable quantumlimited detection with the full accuracy and precision of the frequency comb, avoiding the penalties discussed previously. To achieve these combined advantages, the TPFC is configured as a tracking optical oscillator in time and phase so that it effectively locks onto an incoming weak signal pulse train for coherent signal integration.

As an immediate example, we incorporate the TPFC into a dual-comb ranging system. The result is quantum-limited sensing that sacrifices none of the exquisite accuracy and precision of frequency-comb measurements. Here we show a precision floor of 0.7 nm (4.8 as in time of flight) in ranging, which exceeds previous conventional dual-comb ranging demonstrations<sup>6-8,42-44</sup>. In addition, the tracking dual-comb ranging detects a weak reflected signal-comb pulse train with a mean photon number per pulse of only 1/77 at a sensitivity within a factor of two of the quantum limit. Detection of signals at even lower mean photon per pulse numbers is possible by reducing the measurement bandwidth. In contrast, conventional dual-comb ranging would require a return signal 37 dB or 5,000-times stronger to reach the same level of performance.

The uses of the TPFC go well beyond acting as a tracking optical oscillator. It should enable many more time-based measurement schemes than the conventional vernier approaches using fixed frequency combs. For example, in multi-comb sensing, the relative time offset between the frequency combs can be adjusted to mimic a higher-repetition-rate system while retaining the benefits of a lower-repetition-rate system, for example, higher pulse energy and tight stabilization. Arbitrary patterns can enable future compressive sampling<sup>35</sup>. In time and

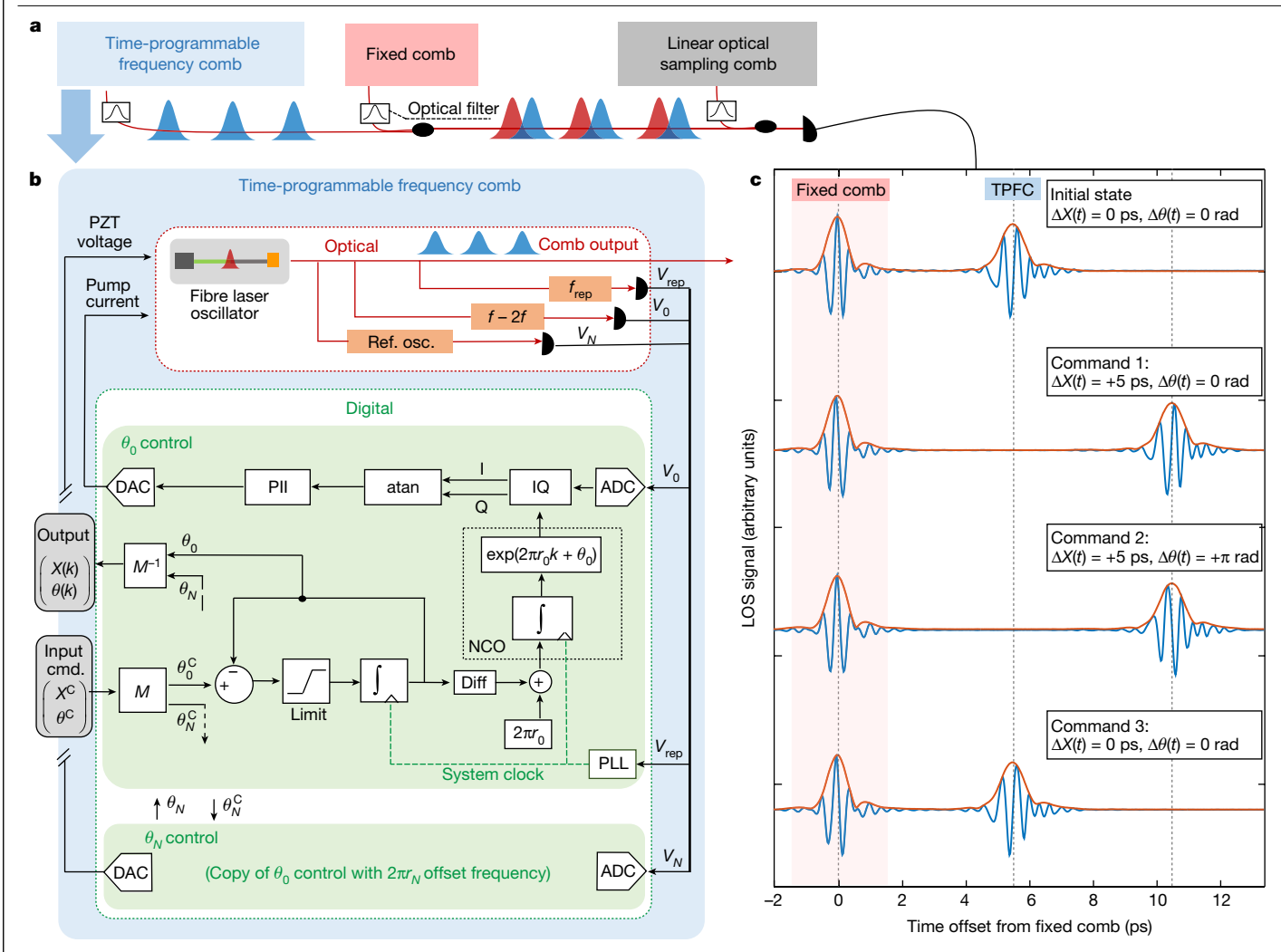


**Fig. 1** | **A time-programmable frequency comb. a**, The TPFC output is measured with respect to a second fixed frequency comb through linear optical sampling (LOS) against a third frequency comb with an offset repetition frequency. The frequency combs operate at  $f_{\rm rep} \approx 200$  MHz with a 5-ns pulse spacing. All pulses are spectrally filtered to a Gaussian 10.1-nm-wide shape, corresponding to 355-fs pulse duration (Methods). b, Schematic of the TPFC. A self-referenced erbium:fibre frequency comb is controlled with digital electronics clocked off the detected comb repetition rate signal ( $V_{\rm rep}$ ). The digital section receives the carrier-envelope offset signal ( $V_0$ ) and the optical beat signal ( $V_N$ ), along with the comb-pulse timing and phase commands,  $X^{\rm C}$  and  $\theta^{\rm C}$ , which are combined to give the control phases  $\theta^{\rm C}_0$  and  $\theta^{\rm C}_N$  through the (trivial) matrix M. These are passed to their respective digital control loop (Methods). The control efforts for  $\theta^{\rm C}_0$  and  $\theta^{\rm C}_N$  adjust the PLLs controlling the

comb's two degrees of freedom. The system tracks the actual phases,  $\theta_0$  and  $\theta_N$ , as fixed-point numbers, which are combined to give the actual pulse timing and phase, X(k) and  $\theta(k)$ , for every comb-pulse number k. ADC, analogue-to-digital converter; cmd, command; DAC, digital-to-analogue converter; Diff, difference operator; IQ, in-phase/quadrature demodulator; NCO, numerically controlled oscillator; PII, proportional-integral-integral controller; PZT, piezo-electric transducer; Ref. osc., reference oscillator;  $r_0$  and  $r_N$ , offset frequencies of the phase locks in units of  $f_{\rm rep}$  (Methods).  ${\bf c}$ , LOS (blue trace) and their envelopes (red trace) for the fixed comb (at X=0) and the TPFC at the given  $(X,\theta)$  values with sequential measurements offset vertically for clarity. The LOS magnification of the time axis is  $10^6$ . Grey dashed vertical lines are provided as a guide to the eye to show alignment of pulse envelope centres across vertically stacked measurements.

frequency metrology, the comb can provide accurately adjustable timing signals, modulation capabilities for noise suppression and optically based time-interval standards<sup>45</sup>. Multiple TPFCs could be used for pump–probe experiments with digital control of pulse spacing replacing delay lines or chirp-induced delays<sup>33</sup>.

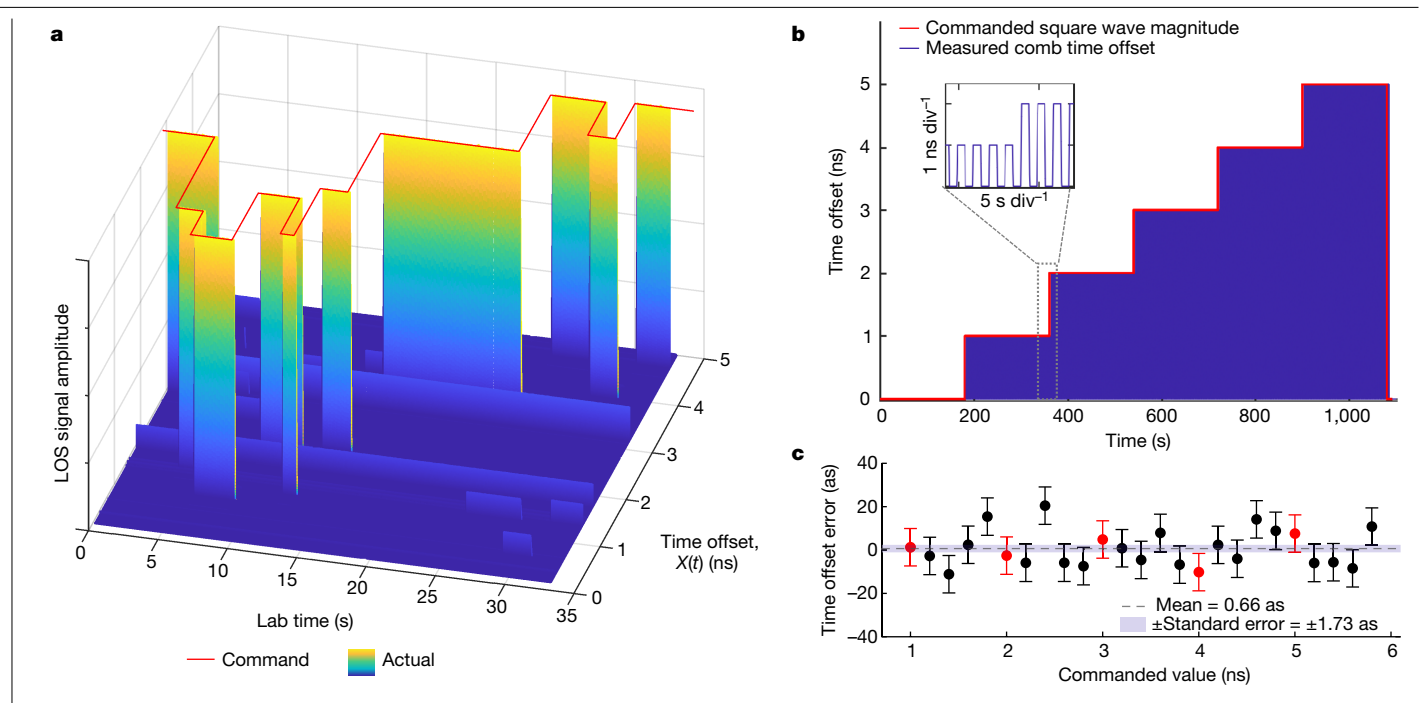
In this paper, we first describe the TPFC and its capabilities generally. We then explore a specific application by integrating the TPFC into a dual-comb ranging system. Finally, we discuss the potential benefits of a TPFC in comb-based sensing more generally, including in LIDAR, spectroscopy and time transfer.

#### The time-programmable frequency comb

The TPFC requires two parts: an optically self-referenced frequency comb and the electronics to track and control the time and phase of the comb

pulses. (See equation (3) for a definition of the time and phase of the comb pulses.) Although the electronic system need not be exclusively digital, it does need to track the programmed comb time and phase at the attosecond level over long (hours to weeks) durations. Here we use a fixed-point number whose least-significant bit corresponds to a less than 1-as shift in time. When combined with an integer pulse number in an 80-bit number, the pulse timing can be specified with zero loss of accuracy for over 1 week at 1-as precision, thereby providing well beyond  $10^{19}$ -level control of the comb timing, commensurate with next-generation optical clocks. As for the comb, any self-referenced comb could be converted into a TPFC; here, we generate a TPFC using a fibre-based comb.

Figures 1 and 2 describe the TPFC and its output characterization. In a self-referenced comb, phase-locked loops (PLLs) stabilize the frequency of the Nth comb tooth,  $f_N$ , with respect to a continuous-wave (CW) reference laser, and the frequency of the 0th comb tooth,  $f_0$ 



 $\label{eq:Fig.2} \textbf{Fig. 2} | \textbf{Illustration and characterization of the time programmability of the TPFC through LOS. a}, The TPFC pulse train, presented as a surface plot, where each slice in lab time represents a complete LOS measurement as in Fig. 1c. Data acquired using the setup in Fig. 1a. The TPFC pulse is located at the LOS signal peak and follows the commanded arbitrary step pattern (red line). Multiple reflections within the set-up appear as small satellite pulses. <math display="block">\textbf{b}, \text{Repeated stepping of the TPFC timing to verify accuracy. Steps are performed at 1 Hz, measured by LOS at 6 kHz (blue line) and the commanded step size (red line) is changed every 3 min. The 1-Hz modulation allows accurate$ 

measurement of the step size by removing fibre-optic path-length drifts. **c**, The error between the actual and commanded pulse times for the data in **b** (red circles). Each point is a 3-min average over about 1 million individual LOS measurements. This measurement was repeated for multiple different commanded time steps (black circles). The uncertainty bars are based on the LOS measurement noise and residual comb timing jitter. The average difference is 0.66 as  $\pm 1.73$  as (standard error). There is no observed reduction in accuracy or precision despite moving the TPFC over the full 5 ns non-ambiguity range.

(the carrier-envelope offset frequency). The PLL locks both frequencies to a known fraction of  $f_{\rm rep}$ , which is self-referentially defined as  $f_{\rm rep} \equiv (f_N - f_0)/N$  (refs.  $^{1.2.4.5}$ ). These PLLs also set the phases of the Nth and 0th comb-tooth frequencies,  $\theta_N$  and  $\theta_0$ , to arbitrary but fixed values. Here we manipulate these phases to control both the comb-pulse phase,  $\theta$ , and the comb-pulse-time offset which is given by  $X = (\theta_0 - \theta_N)/(2\pi N f_{\rm rep})$  in direct analogy to the definition of  $f_{\rm rep}$  above. The digital control exploits the optical frequency division of N inherent to optically self-referenced combs so a single  $2\pi$  shift in the phase of either PLL leads to a time shift of about 5 fs. The TPFC outputs both a train of optical pulses and the corresponding synchronous digital values of pulse time, X, and pulse phase,  $\theta$  (Fig. 1b).

The TPFC is both agile and accurate (Figs. 1c and 2); the output time of a comb pulse can be adjusted arbitrarily. Yet at any instant, we know exactly, to fractions of an optical cycle, by how much the output time (and phase) has been shifted. For rapid changes in the TPFC output, the settling time of the PLLs can be taken into account either through modelling or by including the digital phase error signal from the two PLLs. It is the exactness of the performed step relative to the commanded step (Fig. 2b) and the ability to control the steps in real time that stand in contrast to earlier work. As shown in Fig. 2c, the accuracy of the timing control, X, with respect to the underlying CW reference laser is  $0.66 \pm 1.73$  as.

Here the maximum slew rate between time steps was conservatively set to  $40 \text{ ns s}^{-1}$  to eliminate the possibility of cycle slips in the PLL during motion. The use of an input tracking filter for the PLL signals should enable slew rates as high as  $1 \text{ µs s}^{-1}$ , limited only by the actuators (Methods).

#### Application to dual-comb ranging

To demonstrate the advantages of the TPFC in dual-comb sensing, we consider ranging  $^{6-8}$ . In dual-comb ranging, pulses with bandwidth  $\tau_{\rm p}^{-1}$ 

from a comb are reflected off an object, and their time of flight is detected by heterodyning them against a second comb. This measurement has a resolution of  $\Delta R = c\tau_p/2$ , which characterizes the ability to distinguish two adjacent reflections, where c is the speed of light. It has a non-ambiguity range  $R_{\rm NA} = c/(2f_{\rm rep})$ , associated with 'which pulse' is detected. (This ambiguity can be removed by changing  $f_{\rm rep}$  and repeating the measurement  $^7$ .) The accuracy is set by the comb's reference oscillator or knowledge of the index of refraction. In certain applications, absolute calibration and instability of the reference plane will also factor into the accuracy. The precision is the uncertainty in the peak location of the reflection. At best, the precision is equal to the resolution divided by the signal-to-noise ratio (SNR):

$$\sigma_{\rm R} = \frac{C}{2 \ln(2)} \frac{\Delta R}{\rm SNR_S} \tag{1}$$

where the  $(2\ln(2))^{-1}$  factor arises from assuming Gaussian pulses (Methods). The shot-noise limited SNR SNR<sub>S</sub> =  $\sqrt{\eta n_{\rm s}}$  where  $\eta$  is the detector quantum efficiency and  $n_{\rm s} = P_{\rm rec}T/(hv)$  is the number of signal photons for a received power  $P_{\rm rec}$ , integration time, T, and a photon energy given by the optical frequency, v, and Planck's constant, h. The constant C quantifies how far the precision is from the quantum limit. It can be related to the power penalty as  $P_{\rm p} = C^2$ . An optimal quantum-limited ranging system operates at  $C = P_{\rm p} = 1$ .

Conventional dual-comb ranging operates at a high power penalty and with significant trade-offs. In these systems, the second comb's repetition rate is offset by  $\Delta f_r$  to serve as a linear sampling comb. It repeatedly scans the entire non-ambiguity range,  $R_{\text{NA}}$ , at a measurement rate  $T^{-1} = \Delta f_r \leq f_{\text{rep}} \Delta R/(4R_{\text{NA}})$ . The inherent trade-offs in T,  $R_{\text{NA}}$  and  $\Delta R$  have led to dual-comb ranging implementations using very different frequency combs and covering three orders of magnitude in T and

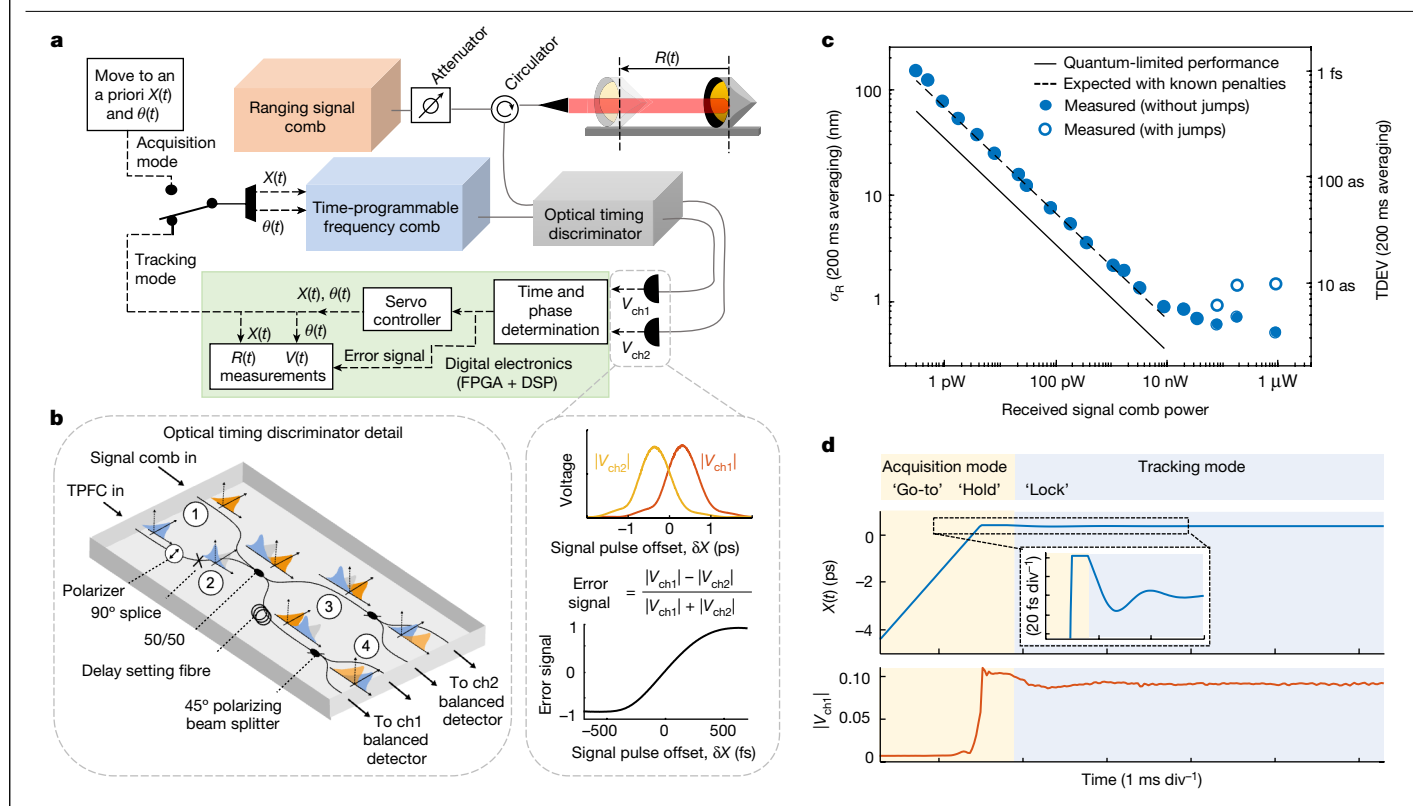


**Fig. 3** | **Dual-comb ranging with a time-programmable frequency comb. a**, System diagram. The TPFC can be run in two modes, acquisition or tracking, as described in the main text. **b**, The timing discriminator is a dual Mach–Zehnder interferometer constructed with polarization-maintaining fibre optics in which (1) both comb pulses enter with the same polarization and (2) the TPFC pulse is rotated to the fast axis. Then (3) the pulses are mixed, a delay between pulses is added to one arm and (4) the pulses are projected back into the same polarization for balanced heterodyne detection to yield the two output signals  $V_{\rm ch1}$  and  $V_{\rm ch2}$ . These signals are demodulated and their magnitudes combined to generate a power-insensitive error signal of the differential comb-pulse-time offset, while their phase yields the differential comb-pulse phase. **c**, Range precision (deviation)  $\sigma_{\rm R}$  (left axis) and

corresponding time deviation TDEV (right axis) at 200-ms averaging time versus the signal-comb power at the balanced photodetectors. The measured precision follows the quantum limit (equation (1)) from  $0.33\pm0.03$  pW to  $10\pm1.0$  nW with a penalty of C=2.16, reaching a systematic noise floor below 1 nm (7 as), which is 2–10 times below previous dual-comb ranging experiments  $^{6-8,42-44}$  and attributed to residual fibre path-length fluctuations. At the three high power points, the deviation is given both for the full data trace and for a subset of the data without approximately 6 sudden ranging/timing jumps of <50-nm amplitude which are attributed to nonlinear optical feedback (and only appear at these higher powers). **d**, Example handover between acquisition and tracking modes. Here the TPFC was commanded to move from X(t) = -5 ps to X(t) = 0 ps where it acquires the signal pulse.

 $\Delta R$  but all facing these strong constraints<sup>6-8,42-44</sup>. Moreover, in all cases, the power penalty  $P_{\rm p} \approx \Delta R/R_{\rm NA} = f_{\rm r} \, \tau_{\rm p}$  is severe, ranging from 14 dB to 38 dB (refs. <sup>7,42</sup>), because of the repeated scanning of the entire non-ambiguity range.

Here, as shown in Fig. 3, we replace the sampling frequency comb by the TPFC to overcome these trade-offs and stiff power penalty. A coherent timing discriminator, shown in Fig. 3b, measures the relative time and phase between the TPFC and signal-comb pulses. Creating two time-shifted copies effectively shapes the TPFC pulse to optimize detection of the time of the incoming signal-comb pulses 46,47. The two heterodyne signals output by the timing discriminator have a nominal carrier frequency of 10 MHz, set by the relative phase locks of the two combs. The signals are then bandpass filtered and demodulated. The choice of bandwidth is a trade-off between update rate and sensitivity. Here, we use 26 kHz to be well above typical roughly kilohertz mechanical vibrations while allowing for a fairly long 38 µs coherent integration time. The amplitudes of the two demodulated signals are combined to compute the time offset between the TPFC and signal comb (Fig. 3b) whereas their phase yields the differential carrier phase of the TPFC and signal-comb pulses whose derivative is the Doppler shift. Critically, the combination of the two channels from the timing discriminator gives a time offset measurement that is independent of the incoming signal power.

This system runs in two modes: acquisition mode and tracking mode, both of which differ from conventional dual-comb ranging.

In acquisition mode, X(t) is scanned until the tracking comb's timing matches the incoming signal pulse train. Although it is possible to scan the entire non-ambiguity range, we can also make use of a priori information to scan the TPFC over much less than the non-ambiguity range. The information could be provided from external sources or from a Kalman filter if previous range and Doppler measurements are available. Once the system acquires the appropriate reflection, it switches to tracking mode (Fig. 3d). Tracking mode implements a pulse-timing lock and a carrier-frequency lock based on the timing discriminator outputs (Methods). The combination of the control and error signals from the time and frequency locks in turn yield the range and Doppler velocity of the target object.

In tracking mode, the ranging precision nearly reaches the quantum limit of equation (1) (Fig. 3c). This nearly quantum-limited precision ranging is demonstrated at a rapid 26-kHz measurement rate with as little as 0.33  $\pm$  0.03 pW of return power (SNR\_s = 9.5), which corresponds to only 1/77 mean photons per pulse. There is a slight penalty of C = 2.16 owing primarily to differential dispersion between the comb pulses (Methods). With additional optimization, C could be reduced to 1, and with squeezing, to less than 1 (ref.  $^{46}$ ). With these same 200-MHz combs, conventional dual-comb ranging would suffer from a power penalty  $P_{\rm p}$  = 37 dB (C = 71). Finally, momentary loss of signal is not an issue. If brief enough that the object position does not differ from prediction, for example, from a Kalman filter, by more than about  $\pm 2\Delta R \approx \pm 100~\mu{\rm m}$ ,

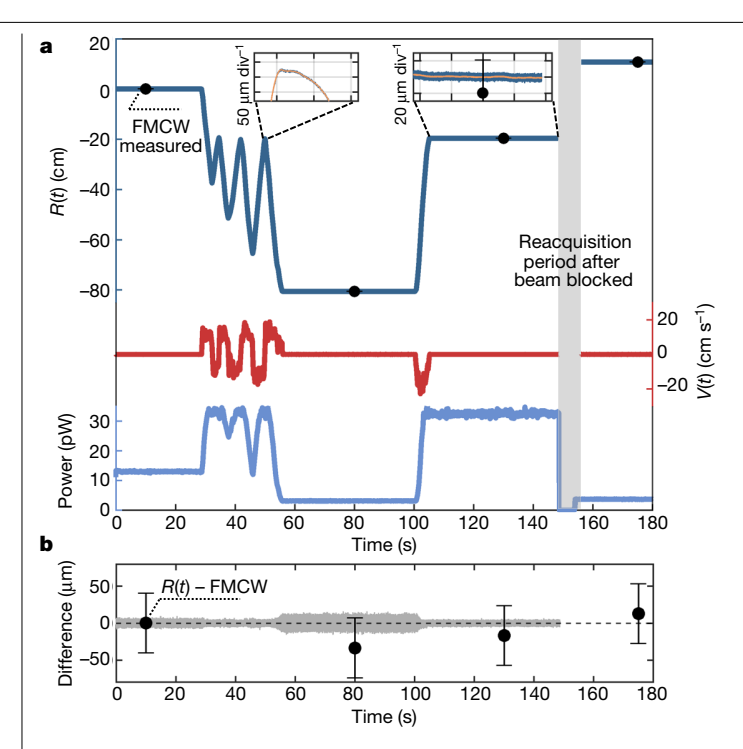


Fig. 4 | Ranging and velocity data to a moving retroreflector. a, The range (top left axis, dark blue trace) is measured from the summed control and error signals for X(t) in tracking mode at a 26-kHz rate. The velocity (right middle axis, red trace) is calculated from summed control and error signals for  $d\theta(t)/dt$ . At 150 s, the beam was blocked and the target moved, triggering a re-acquisition. Before and after re-acquisition, the measured range agrees with a commercial FMCW ranging system (black circles), to within the FMCW uncertainty driven by target vibrations (Methods). The relative range also agrees well with the interferometric range from the unwrapped carrier phase (yellow trace in the two insets), after applying an overall offset. **b**, Difference between the dualcomb range and FMCW range (black circles) and between the dual-comb range and interferometric range from the unwrapped carrier phase for the initial section with continuous signal (grey trace). The range deviation of this latter difference reaches 10 nm and 5 nm at 10-s averaging for the time periods with received powers of  $3.2 \pm 0.3$  pW and  $32 \pm 3.0$  pW, respectively (Extended Data Fig. 1).

tracking simply resumes. For even a 10g acceleration, an approximately 1.5-ms-duration loss of signal is tolerable. Sometimes the signal loss may be too long, for example, in strong air turbulence<sup>48</sup>, in which case the system can transition to acquisition mode using previous data to limit the scan, as discussed above.

Figure 4 shows range data taken while moving the rail-mounted retroreflector. The dual-comb system tracks the retroreflector as it reverses direction at velocities up to 20 cm s<sup>-1</sup>. The signal is blocked at 150 s and the retroreflector moved, after which the absolute range was reacquired by scanning over a ±37.5-cm window. For validation, we compare with a commercial frequency-modulated continuous-wave (FMCW) system at a few static rail positions after calibrating out differential range offsets. The two agree to within the FMCW measurement uncertainty of ±40 µm owing to target vibrations amplified by the FMCW's intrinsic range-Doppler coupling (Extended Data Fig. 2). Finally, the coherent timing discriminator also outputs the relative carrier phase between the signal comb and TPFC, whose derivative yielded the velocity above. This phase can also be unwrapped to provide relative range during periods of continuous signal (Fig. 4a, yellow trace) as in ref. <sup>7</sup> and similar to CW interferometry (except avoiding systematic errors from spurious reflections). This unwrapped carrier phase agrees with the tracking range to a precision limited by the tracking range noise which follows equation (1), after accounting for an

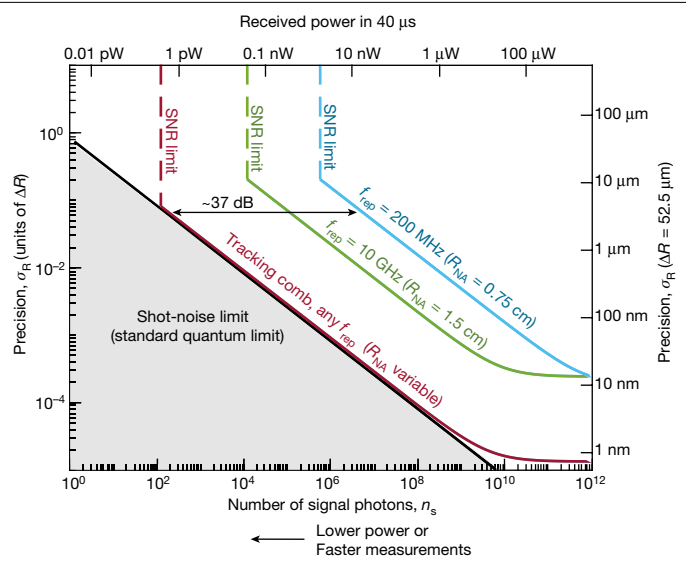


Fig. 5 | Comparison of conventional and tracking dual-comb ranging. Precision versus received signal photons,  $n_s = SNR_s^2/\eta$ , for conventional dualcomb ranging at  $f_{rep} = 200$  MHz (blue line) and  $f_{rep} = 10$  GHz (green line), compared with tracking dual-comb ranging (red line) and the standard quantum limit for heterodyne detection (black line). The left and bottom axes are in normalized units whereas the right and top axes are scaled to values similar to those used in this work. For conventional dual-comb ranging, the scaling depends strongly on  $f_{rep}$  and the precision is always much worse than the standard quantum limit. The tracking dual-comb ranging (red line) is independent of  $f_{rep}$  and can reach the standard quantum limit, although here shown with a 10% penalty. We assume a system noise floor of 0.7 nm, taken from this work, for the tracking comb, and about 10 nm for the conventional dualcomb systems<sup>7,42</sup>. For all three ranging configurations, we require a minimum detection SNR of about 10 for reasonable detection statistics, as indicated by the SNR limit. The 37-dB improvement, however, is independent of this chosen limit.

approximately 1.5-times chirp-induced penalty in C from the fibre-optic path to reach the rail system.

#### Broader benefits to comb-based sensing

A number of existing or potential applications should benefit from the abilities illustrated in Figs. 1-3, specifically to (1) set the time and phase of the comb's output pulses, (2) coherently scan the relative temporal spacing between two frequency combs over a specified limited range rather than the full inverse repetition rate, thereby mimicking a higher-repetition-rate comb while avoiding limitations of lower pulse energy, and (3) operate as a precision optical tracking oscillator in time and frequency for shot-noise limited sensing. Below we discuss three different general application areas: LIDAR, time metrology and spectroscopic sensing.

As already discussed, frequency combs have a natural connection to precision LIDAR. Figure 5 and Extended Data Table 1 together compare conventional dual-comb ranging<sup>7,42-44</sup>, tracking dual-comb ranging and FMCW ranging<sup>49</sup>, which is the standard approach to high-resolution optical ranging. For all three, the resolution is set by the optical bandwidth and the accuracy by the comb referencing or knowledge of the index of refraction of air. (Comb-assisted FMCW ranging can transfer frequency-comb accuracy to FMCW LIDAR<sup>50</sup>.) Both tracking dual-comb ranging and FMCW ranging can reach the shot-noise limit and exploit the optical carrier phase. However, the update rate of FMCW ranging is limited by the laser sweep time and its uncertainty can be degraded by target vibrations. Tracking dual-comb ranging avoids vibration-related systematics. It could

provide range-resolved vibrometry in a cluttered environment or surface imaging through turbulent media even with speckle-induced dropouts and high loss. (A 10-mW launch power will still provide sufficient 1-pW return power to enable a 26-kHz measurement rate given a –100-dB reflection.) More generally, there are strong overlaps with conventional radiofrequency pulse-Doppler radar and the tracking comb could therefore have interesting applications to high-bandwidth synthetic aperture LIDAR<sup>51</sup>.

In time-frequency metrology, a TPFC phase-locked to an optical atomic clock provides an optical timescale with the ability to 'adjust' its output time to synchronize with other signals. A TPFC could also enable calibration of time-interval counters<sup>45</sup>. The time-interval standard would follow Fig. 1c, where the TPFC allows precisely defined variable pulse spacing from nanoseconds to femtoseconds. This offers the prospect of a time-interval standard that spans six orders of magnitude with attosecond precision and an accuracy directly tied to a secondary representation of the second. For absolute optical frequency measurements, the TPFC also enables determination of the mode number N by applying a shift  $\Delta\theta_0 = 2\pi N$ , which will lead to a time shift of exactly  $\Delta X = f_{\text{rep}}^{-1}$  for the correct N. Any integer error in N appears as a multiple of 5-fs offset in time, which can be resolved with a second comb and a timing discriminator. In secure optical communications, the programmable comb might enable quadrature pulse phase-position modulation if implemented with high-speed actuators. Finally, the TPFC has interesting applications to comb-based long-distance free-space time transfer<sup>13-17,19,20,23,48</sup> as it provides similar advantages as in dual-comb ranging52.

The TPFC can also break trade-offs that limit comb-based linear and nonlinear spectroscopy. Relatively low-repetition-rate frequency combs (100 MHz to 1 GHz) provide the high pulse energies needed for nonlinear spectroscopy or for spectrally broadening over the desired spectral band<sup>53–55</sup>. However, the spectral resolution set by these low repetition rates is often poorly matched to the application leading to significant 'dead time' or SNR reduction in multi-comb-based spectroscopy<sup>24,26–31,54,55</sup>. The TPFC can circumvent this problem by coherently scanning over a limited time offset between two or more frequency combs, as demonstrated incoherently in the early dual-comb spectroscopic work of ref. 38. In this way, a low-repetition-frequency TPFC can act as a frequency comb with an effectively much higher repetition rate, set by the inverse of the temporal scan window, at shot-noise-limited sensitivity. Going further, the ability to jump the frequency comb-pulse phase and timing could enable compressive sampling in dual-comb or multi-comb sensing applications with a concomitant increase in measurement rate. Recent modelling<sup>35</sup> and preliminary experiments<sup>34</sup> have highlighted the advantages of this dynamic control for dual-comb spectroscopy. Finally, in nonlinear spectroscopy, temporal control could enable time-ordered multi-photon excitation, following the comb-based spectroscopy of rubidium<sup>33</sup> but with programmable control.

#### Conclusion

The TPFC combines the precision and accuracy of a self-referenced frequency comb with flexibility in time and phase and 2-as accuracy. Here the TPFC is based on a fibre frequency comb, but any self-referenced comb (or comb locked to widely separated optical oscillators) with control electronics capable of tracking and manipulating phase could act as a TPFC. Through a dual-comb ranging demonstration, we show the TPFC can operate as an optical tracking oscillator in time and frequency, yielding nearly quantum-noise-limited ranging with 0.7-nm precision. Finally, dual-comb ranging is just one application and the TPFC has equal promise in relaxing trade-offs with repetition frequency and improving SNR in other multi-comb sensing and metrology applications while retaining the hallmark accuracy of comb-based metrology.

#### **Online content**

Any methods, additional references, Nature Research reporting summaries, source data, extended data, supplementary information, acknowledgements, peer review information; details of author contributions and competing interests; and statements of data and code availability are available at https://doi.org/10.1038/s41586-022-05225-8.

- . Hänsch, T. W. Nobel Lecture: Passion for precision. Rev. Mod. Phys. 78, 1297-1309 (2006).
- Hall, J. L. Nobel Lecture: Defining and measuring optical frequencies. Rev. Mod. Phys. 78, 1279–1295 (2006).
- Newbury, N. R. Searching for applications with a fine-tooth comb. Nat. Photon. 5, 186–188 (2011).
- Fortier, T. & Baumann, E. 20 years of developments in optical frequency comb technology and applications. Commun. Phys. 2, 153 (2019).
- Diddams, S. A., Vahala, K. & Udem, T. Optical frequency combs: coherently uniting the electromagnetic spectrum. Science 369, eaay3676 (2020).
- 6. Zhu, Z. & Wu, G. Dual-comb ranging. Engineering 4, 772–778 (2018).
- Coddington, I., Swann, W. C., Nenadovic, L. & Newbury, N. R. Rapid and precise absolute distance measurements at long range. Nat. Photon. 3, 351–356 (2009).
- Kim, W. et al. Absolute laser ranging by time-of-flight measurement of ultrashort light pulses. J. Opt. Soc. Am. A 37, B27-B35 (2020).
- Minoshima, K. & Matsumoto, H. High-accuracy measurement of 240-m distance in an optical tunnel by use of a compact femtosecond laser. Appl. Opt. 39, 5512–5517 (2000).
- Vicentini, E., Wang, Z., Van Gasse, K., Hänsch, T. W. & Picqué, N. Dual-comb hyperspectral digital holography. Nat. Photon. 15, 890–894 (2021).
- Kato, T., Uchida, M. & Minoshima, K. No-scanning 3D measurement method using ultrafast dimensional conversion with a chirped optical frequency comb. Sci. Rep. 7, 3670 (2017).
- Hase, E. et al. Scan-less confocal phase imaging based on dual-comb microscopy. Optica 5, 634–643 (2018).
- Deschênes, J.-D. et al. Synchronization of distant optical clocks at the femtosecond level. Phys. Rev. X 6, 021016 (2016).
- Giorgetta, F. R. et al. Optical two-way time and frequency transfer over free space. Nat. Photon. 7, 434–438 (2013).
- Xin, M., Şafak, K. & Kärtner, F. X. Ultra-precise timing and synchronization for large-scale scientific instruments. Optica 5, 1564–1578 (2018).
- Shen, Q. et al. Experimental simulation of time and frequency transfer via an optical satellite-ground link at 10<sup>-18</sup> instability. Optica 8, 471–476 (2021).
- Boulder Atomic Clock Optical Network (BACON) Collaboration Frequency ratio measurements at 18-digit accuracy using an optical clock network. Nature 591, 564–569 (2021)
- Clivati, C. et al. Common-clock very long baseline interferometry using a coherent optical fiber link. Optica 7. 1031–1037 (2020).
- Bergeron, H. et al. Femtosecond time synchronization of optical clocks off of a flying quadcopter. Nat. Commun. 10, 1819 (2019).
- Bodine, M. I. et al. Optical time-frequency transfer across a free-space, three-node network. APL Photon. 5, 076113 (2020).
- Dix-Matthews, B. P. et al. Point-to-point stabilized optical frequency transfer with active optics. Nat. Commun. 12, 515 (2021).
- Gozzard, D. R. et al. Ultrastable free-space laser links for a global network of optical atomic clocks. Phys. Rev. Lett. 128, 020801 (2022).
- Shen, Q. et al. 113 km free-space time-frequency dissemination at the 19th decimal instability. Preprint at https://arxiv.org/abs/2203.11272 (2022).
- Coddington, I., Newbury, N. & Swann, W. Dual-comb spectroscopy. Optica 3, 414–426 (2016).
- Cossel, K. C. et al. in Advances in Spectroscopic Monitoring of the Atmosphere (eds Chen, W. et al.) 27–93 (Elsevier, 2021); https://doi.org/10.1016/B978-0-12-815014-6.00008-7.
- Picqué, N. & Hänsch, T. W. Frequency comb spectroscopy. *Nat. Photon.* 13, 146–157 (2019).
- Lomsadze, B., Smith, B. C. & Cundiff, S. T. Tri-comb spectroscopy. *Nat. Photon.* 12, 676–680 (2018).
- Friedlein, J. T. et al. Dual-comb photoacoustic spectroscopy. Nat. Commun. 11, 3152 (2020).
- Wildi, T., Voumard, T., Brasch, V., Yilmaz, G. & Herr, T. Photo-acoustic dual-frequency comb spectroscopy. Nat. Commun. 11. 4164 (2020).
- Ideguchi, T. et al. Coherent Raman spectro-imaging with laser frequency combs. Nature 502, 355–358 (2013)
- Rieker, G. B. et al. Frequency-comb-based remote sensing of greenhouse gases over kilometer air paths. Optica 1, 290–298 (2014).
- Voumard, T. et al. Al-enabled real-time dual-comb molecular fingerprint imaging. Opt. Lett. 45, 6583–6586 (2020).
- Marian, A., Stowe, M. C., Lawall, J. R., Felinto, D. & Ye, J. United time-frequency spectroscopy for dynamics and global structure. Science 306, 2063–2068 (2004)
- Giorgetta, F. R. et al. Fiber laser based dual-comb spectroscopy with dynamically controlled spectral resolution. In Conference on Lasers and Electro-Optics (2021) AM3E.4 (Optical Society of America, 2021).
- Kawai, A., Kageyama, T., Horisaki, R. & Ideguchi, T. Compressive dual-comb spectroscopy. Sci. Rep. 11. 13494 (2021).
- Martin, B., Feneyrou, P., Dolfi, D. & Martin, A. Performance and limitations of dual-comb based ranging systems. Opt. Express 30, 4005 (2022).
- Ellis, J. L. et al. Scaling up frequency-comb-based optical time transfer to long terrestrial distances. Phys. Rev. Appl. 15, 034002 (2021).

- Schliesser, A., Brehm, M., Keilmann, F. & van der Weide, D. Frequency-comb infrared spectrometer for rapid, remote chemical sensing. Opt. Express 13, 9029-9038 (2005).
- 39. Tourigny-Plante, A., Guay, P. & Genest, J. Apodization in dual-comb spectroscopy for rapid measurement. In Optical Sensors and Sensing Congress (2020) LTu3C.2 (Optical Society of America, 2020).
- 40. Shi, Y. et al. High speed time-of-flight displacement measurement based on dual-comb electronically controlled optical sampling. Opt. Express 30, 8391-8398 (2022).
- 41. Antonucci, L., Solinas, X., Bonvalet, A. & Joffre, M. Asynchronous optical sampling with arbitrary detuning between laser repetition rates. Opt. Express 20, 17928-17937 (2012).
- Trocha, P. et al. Ultrafast optical ranging using microresonator soliton frequency combs. Science 359, 887-891 (2018).
- 43. Mitchell, T., Sun, J., Sun, J. & Reid, D. T. Dynamic measurements at up to 130-kHz sampling rates using Ti:sapphire dual-comb distance metrology. Opt. Express 29, 42119-42126
- Suh, M.-G. & Vahala, K. J. Soliton microcomb range measurement, Science 359, 884-887 44. (2018).
- 45. Kalisz, J. Review of methods for time interval measurements with picosecond resolution. Metrologia 41, 17-32 (2004).
- 46. Fabre, C. & Treps, N. Modes and states in quantum optics, Rev. Mod. Phys. 92, 035005 (2020).
- 47. Ansari, V. et al. Achieving the ultimate quantum timing resolution. PRX Quantum 2, 010301 (2021)
- 48. Sinclair, L. C. et al. Synchronization of clocks through 12 km of strongly turbulent air over a city. Appl. Phys. Lett. 109, 151104 (2016).

- 49. Barber, Z. W., Dahl, J. R., Sharpe, T. L. & Erkmen, B. I. Shot noise statistics and information theory of sensitivity limits in frequency-modulated continuous-wave ladar. J. Opt. Soc. Am. A 30, 1335-1341 (2013).
- 50. Baumann, E. et al. Comb-calibrated frequency-modulated continuous-wave ladar for absolute distance measurements. Opt. Lett. 38, 2026-2028 (2013).
- Crouch, S. & Barber, Z. W. Laboratory demonstrations of interferometric and spotlight synthetic aperture ladar techniques. Opt. Express 20, 24237 (2012).
- Caldwell, E. D. et al. Photon efficient optical time transfer. In 2022 Joint Conference of the European Frequency and Time Forum & the IEEE International Frequency Control Symposium Paris, France (2022).
- 53. Schliesser, A., Picqué, N. & Hänsch, T. W. Mid-infrared frequency combs. Nat. Photon. 6, 440-449 (2012).
- 54. Ycas, G. et al. High-coherence mid-infrared dual-comb spectroscopy spanning 2.6 to 5.2 μm. Nat. Photon. 12, 202-208 (2018).
- 55. Muraviev, A. V., Smolski, V. O., Loparo, Z. E. & Vodopyanov, K. L. Massively parallel sensing of trace molecules and their isotopologues with broadband subharmonic mid-infrared frequency combs. Nat. Photon. 12, 209-214 (2018).

Publisher's note Springer Nature remains neutral with regard to jurisdictional claims in published maps and institutional affiliations.

© This is a U.S. Government work and not under copyright protection in the US; foreign copyright protection may apply 2022

### **Methods**

#### **TPFC** control

The output of the frequency comb can be written as a function of time, t, in terms of a sum of pulses, labelled by integer k, with repetition frequency  $f_{\text{ren}}$ 

$$E(t) = e^{-i\theta} \sum_{k} E_{k}(t - X)$$
where  $E_{k}(t) = e^{-ik\theta_{ceo}} A(t - kf_{rep}^{-1})$  (2)

where  $\theta$  and X are the comb-pulse phase and time offset (to be controlled later), A is the pulse amplitude, and  $\theta_{ceo}$  is the carrier-to-envelope phase advance per pulse (and hence appears as  $k\theta_{ceo}$ ) and is not to be confused with  $\theta$ . Alternatively, through the Poisson sum formula, the comb can be written as

$$E(t) = f_{\text{rep}} e^{-i\theta} \sum_{n} \widetilde{A}_{n} e^{-i2\pi i f_{n}(t-X)}, \tag{3}$$

where *n* is the index of the comb tooth with complex amplitude  $\widetilde{A}_n$  at frequency  $f_n = nf_{\text{rep}} + f_0$  and the carrier-envelope offset frequency  $f_n = (2\pi)^{-1}\theta_{\text{tot}}$ .

 $f_0 = (2\pi)^{-1}\theta_{\rm ceo}^n f_{\rm rep}^{-1}$ . For a comb self-referenced to a reference CW laser, we stabilize the comb-tooth frequencies,  $f_0$  and  $f_N$ , where N is the tooth nearest the reference CW laser at  $f_{\rm CW}$ . Each of these frequencies is stabilized with respect to the repetition frequency, that is,  $f_0 = r_0 f_{\rm rep}$  and  $f_N = f_{\rm CW} - r_N f_{\rm rep}$ , where both  $r_0$  and  $r_N$  are user-chosen rational fractions. It is noted that the repetition rate itself is determined by the two frequencies as  $f_{\rm rep} = (f_N - f_0)/N$ . Equivalently,  $f_{\rm rep} = f_{\rm CW}/(N + r_0 + r_N)$ . This stabilization is done through two PLLs that combined also set the overall phase,  $\theta$ , and time offset, X, to arbitrary but fixed values. If the phase and time offset were not fixed, variation in X would lead to an effective variation in the repetition frequency  $f_{\rm rep}$ , and variation in  $\theta$  would similarly lead to a variation in  $\theta_{\rm ceo}$ .

Here we alter the lock points of the two PLLs to coherently change the overall phase,  $\theta$ , and time offset, X. Consider the phase lock of the tooth at n=0 (that is, the carrier-envelope offset stabilization). The phases satisfy the equation

$$[\theta + 2\pi f_0 t - 2\pi f_0 X] - r_0 [2\pi f_{\text{ren}} t - 2\pi f_{\text{ren}} X] - \theta_{0,\text{cal}} = 0$$
 (4)

where the first term in brackets is the phase of the n=0 term in equation (3) assuming an unchirped A(t). The second term in brackets is the phase of the repetition signal, that is the digital clock signal for the digital PLL that directly follows the detected comb-pulse arrival times. The final term is a calibration offset related to the difference in the total phase delays of the two signals up to the in-phase/quadrature (IQ) demodulation (phase comparison). In the standard fixed comb control, feedback is applied to drive this phase difference to zero, as indicated by the right-hand side of the equation. With synchronous digital electronics, we can replace the right-hand side with a time-dependent control phase,  $\theta_0^{\rm C}(t)$ . As  $f_0 \equiv r_0 f_{\rm rep}$ , equation (4) reduces to

$$\theta(t) = \theta_0^{C}(t) \tag{5}$$

after dropping the calibration constant for simplicity. We apply the same arguments to the phase of the n = N tooth, working from the stabilization of  $f_N = f_{CW} - r_N f_{rep}$  to find

$$\theta(t) - 2\pi(N + r_0 + r_N) f_{\text{rep}} X(t) = \theta_N^{C}(t).$$
 (6)

A linear combination of equations (4) and (5) (represented by the matrix  $M^{-1}$  in Fig. 1) gives us the simple relationships

$$\theta(t) = \theta_0^{C}(t)$$

$$X(t) = \frac{\theta_0^{C}(t) - \theta_N^{C}(t)}{2\pi f_{CW}}$$
(7)

These equations relate changes in the time-varying control phases to the comb-pulse phase and timing. They hold within the feedback bandwidth of the PLL. (In practice, we can change the signal more rapidly provided we separately record the error signal quantifying the difference between the set point and actual values). For the particular locking conditions chosen here of  $r_N = -r_0$ , these equations reduce to the ones given in the main text. To set the TPFC output, the inverse of equation (6) generates the desired values of  $\theta_0^{\rm C}(t)$  and  $\theta_N^{\rm C}(t)$ , which are then translated to the actuator controls. (See Fig. 1 and below for details on processing).

With appropriate choice of the control phases, we can control the comb's time offset and phase, or the phase of a particular tooth through equation (7). The phase change of the *n*th tooth is

$$\theta_{n}(t) = \theta(t) - 2\pi f_{n} X$$

$$= \left(1 - \frac{n + r_{0}}{N + r_{0} + r_{N}}\right) \theta_{0}^{C}(t) + \frac{n + r_{0}}{N + r_{0} + r_{N}} \theta_{N}^{C}(t)$$
(8)

For the tracking comb operation, we adjust  $\theta_0^C$  and leave  $\theta_N^C = 0$ . This leads to a time shift of  $\Delta X = \Delta \theta_0^C/(2\pi N f_{\rm rep})$  when keeping the phase of the Nth comb tooth to zero as the timing of the TPFC comb pulses is shifting. As a result, the relative phase shift of the Nth comb tooth between the TPFC and signal comb reflects the overall additional phase shift on the signal comb alone. Therefore, in 'unwrapping' the phase of the carrier signal measured during the retroreflector motion, we must use an effective carrier frequency of  $N f_{\rm rep}$ .

#### Hardware and digital electronic system

Frequency combs. The fibre-based frequency combs used in this work operate at a repetition frequency of about 200 MHz and are based on the design in ref. <sup>56</sup>. The actuator for the carrier-envelope-offset phase lock is the oscillator pump power and the actuators for the lock of the *N*th comb tooth to the optical reference are two piezo-electric fibre stretchers, which together adjust the oscillator cavity length. All combs are housed within temperature-controlled enclosures. The output of all combs are filtered with a 10.1-nm-wide Gaussian filter centred at 1,560 nm, resulting in 5 mW of in-band power, which was often strongly attenuated for these experiments. The optical reference for all combs is a cavity-stabilized laser at 1,535.04 nm. To minimize excess residual noise between the frequency combs, all non-common fibre lengths between the cavity-stabilized laser and the three combs are as short as possible and contained within the temperature-controlled housing as much as possible.

To produce the required heterodyne signals between the TPFC, fixed comb and linear optical sampling (LOS) comb pulses, fibre-optic-based optical transceivers were constructed with polarization-maintaining fibre optics (PM-1550) and fibre-optic components. The fibre-optic-based timing discriminator described in Fig. 1 was constructed with a differential path length of 50.5 cm of fibre, which corresponds to a 980-fs delay between the lead and lag arms to match the full-width at half-maximum (FWHM) of the partially chirped cross-correlation (or interferogram) signal between the tracking and signal frequency combs. Commercial 100-MHz balanced detectors are used throughout, including at the output of the timing discriminator, to allow for shot-noise-limited heterodyne detection with about 1.1-dB power penalty.

For the data in Figs. 1c and 2, we combine a fixed comb and a TPFC, both phase-locked with the same values of N,  $r_0$  and  $r_N$ . We then adjust the TPFC pulse time or phase, and subsequently probe the relative

phase and time between the TPFC and the fixed comb through a third LOS frequency comb. For the data in Figs. 3 and 4, we do not use the third frequency comb. In all cases, the LOS comb is phase-locked to the same CW reference laser but with its carrier frequency offset by 10 MHz. The heterodyne signal between the LOS and the other two combs is digitized at  $f_{\text{rep,LOS}}$  yielding an interferogram with  $f_{\text{rep,LOS}}/\Delta f_{\text{rep}}$ points. For the data in Figs. 1c and 2a, the LOS comb was offset in repetition frequency by about 200 Hz whereas for the data in Fig. 2b (which required faster averaging), the LOS comb was offset in frequency by about 6 kHz, very near the Nyquist limit for LOS given the pulse width. For Fig. 2b, we additionally apply a matched filter before peak fitting. In these LOS sampled measurements, the overlap between the LOS combs and the TPFC is sufficiently short that the full timing jitter of the relative comb pulses is measured. For these combs, this timing jitter was about 3 fs. For the data in Fig. 2b, multiple measurements allow us to average down this jitter. At these longer averaging times, differential out-of-loop fibre paths in the TPFC and LOS combs will lead to slow femtosecond-level time wander. We cancel some of this wander by applying the square-wave 1-Hz modulation to the TPFC time offset.

Timing discriminator. In contrast to the LOS sampling method, the combination of the TPFC and timing discriminator provides continuous measurements at each comb pulse. Low-pass filtering rejects most of the technical timing jitter on the comb pulses that occurs at about 50 kHz (the PLL locking bandwidth). The data for Fig. 3c and Extended Data Fig. 1 were acquired using this continuous timing comparison between the reflected signal frequency comband TPFC. For these data, the signal-comb pulses were reflected off a fibre FC/PC (ferrule connector/physical contact) connector end located just outside the aluminium box that housed the two combs to minimize temperature-induced path-length changes or the even larger atmospheric fluctuations that occur over the air path to the retroreflector.

Ranging set-up. For the ranging data in Fig. 4, the retroreflector on the rail was aligned with three passes so that the effective path-length change and Doppler shift of the comb pulses were a factor of three higher than that of the reflector itself. The signal-comb light was attenuated significantly before launch to reach the low-picowatt-power levels. The position of the retroreflector on the rail was simply adjusted by hand in an arbitrary pattern. The alignment of the output signal-comb light to the retroreflector was not perfect, leading to the power variations in the return signal observed in Fig. 4.

At each static location, a commercial FMCW ranging system took 25 range profiles over a 10-s acquisition period. The reported FMCW range in Fig. 4 is the average of the peak values extracted by a three-point cubic spline fit of the peak. The uncertainty was generated by performing the same fitting routine over 10 min of static range data and taking the standard deviation of the resultant ranges. For both the dual-comb system and FMCW system, the range was calculated using the group velocity calculated at the centre frequency. The large uncertainty on the FMCW range values is owing to the systematic coupling between range and velocity in this frequency-domain ranging system. For the FMCW ranging system used here with a 12.5 THz s<sup>-1</sup> sweep rate, the systematic ranging error is 12  $\mu$ m ×  $\delta f_{\text{Doppler}}$ , where  $\delta f_{\text{Doppler}}$  is the vibration-induced Doppler shift. Although Doppler shifts slower than the sweep rate can be compensated through the use of up and down sweeps, vibration-induced Doppler shifts on timescales comparable to the sweep time cannot be similarly cancelled, leading to the uncertainty bars on the FMCW ranging data in Fig. 4. The tracking dual-comb ranging does not suffer from this strong Doppler-induced systematic error as the ambiguity function for a pulse does not have the large delay-Doppler coupling of a slow FMCW sweep.

**Digital platform.** The implementation of the digital control of the TPFC was accomplished using available hardware and consists of two

field-programmable gate arrays (FPGAs) and one digital signal processor (DSP), although these FPGAs and DSP could be combined into a single platform as the processing load is not significantly larger than fixed comb control. The FPGAs are both clocked synchronously at the comb repetition rate and the DSP processes samples synchronously at exactly 5,000 times slower (about 40 kHz). As the DSP is programmed in C++, it provides a more flexible development environment than the FPGAs. The fixed and LOS frequency combs also each had a dedicated FPGA $^{56}$  for their phase-locking to the CW reference laser.

**Timing and phase commands.** To control the TPFC output, equation (6) generates the desired values of  $\theta_0^C(t)$  and  $\theta_N^C(t)$ . (It is noted that these are 'unwrapped' quantities and are not restricted to a 0 to  $2\pi$  range). In the implementation, all phase and frequencies are defined with respect to the clock cycles of the analogue-to-digital converters, FPGAs and DSP that are synchronous with the instantaneous comb repetition frequency. Within the FPGA, the values of  $\theta_0^C(t)$  and  $\theta_N^C(t)$  can be represented as large fixed-point values such that there is no quantization noise variation across the full range (such as would be inevitable with floating points). Here we use a least-significant bit that corresponds to a comb timing step of below 1 as. All values are then otherwise exact and set with subcycle accuracy, assuming no cycle slips in any clock signal, which is assured by the high-SNR signal from the photo-detected frequency-comb-pulse train.

Figure 1b shows the effective implementation for the phase trajectories for  $\theta_0(t)$  and  $\theta_N(t)$ . The implementation is done through the numerical integration of a limited difference between desired and actual trajectories. This allows enforcing rate limiting to respect the limits of the physical system, for example, the maximum rate that the system can change pulse timing via pump power or cavity length. The phase change is done by changing the effective values of  $r_0$  and  $r_N$  for a precisely known time period inside the FPGA. The commands for setting the trajectories can be sent via either a graphical user interface from a PC, via a serial port input from another real-time digital system for tighter control (for example, the DSP). It could also be done via a sequencer running directly on the control FPGA, although that approach was not used for this study. The rest of the control algorithm for the phase locks is a proportional-integral-integral controller (PII) with a phase extraction front-end, as in ref. <sup>56</sup>.

**Slew rate.** For large time steps, the TPFC response will be limited by the maximum slew rate. A linear slew of the comb-pulse time corresponds to a frequency shift of the phase-locked  $f_0$  or  $f_N$  frequencies (where the latter is measured by its heterodyne beat signal against the CW reference laser). For a frequency shift of  $\Delta f$  in either of these frequencies, the slew rate is  $\mathrm{d}X/\mathrm{d}t \approx \Delta f/f_N$ . Typically, comb actuators can move either of these frequencies by a few modes (for example, through the pump current modulation or cavity fibre stretcher). In that case,  $\Delta f \approx \pm f_{\mathrm{rep}}/f_N$  giving a slew rate of  $\mathrm{d}X/\mathrm{d}t \approx f_{\mathrm{rep}}/f_N$ . For the frequency combs used here, this yields a maximum potential slew rate of  $\mathrm{d}X/\mathrm{d}t \approx 200 \,\mathrm{MHz}/200 \,\mathrm{THz} = 1 \,\mathrm{\mu s} \,\mathrm{s}^{-1}$ .

To maintain the full accuracy of the comb, there is a second potential constraint to the maximum slew rate. Namely, despite a shift in either of the beat frequencies,  $f_0$  or  $(f_N - f_{\rm CW})$ , the system must reliably track the phase of both beat signals; any cycle slip would result in a loss of accuracy for both the comb-pulse time and phase. The resulting limitation on the slew rate depends on a combination of the SNR of the relevant beat signal and sophistication of the demodulation scheme. Indeed, with very high SNR, the beats can be tracked over the full Nyquist window of 0 to  $\pm f_{\rm rep}/2$  and there is no additional limitation. For a typical SNR, one could implement a tracking filter with feedforward to track dynamic frequency changes and avoid cycle slips even with large deviations in the beat frequency. This approach should minimize any slew-rate limitations. However, we did not implement such a filter here. As a result, in the current system, we limited the maximum slew rate to

 $40 \text{ ns s}^{-1}$ . This rate was not optimized but was chosen conservatively to avoid cycle slips, which was verified experimentally. The  $40 \text{ ns s}^{-1}$  slew rate was used for the data in Figs. 1 and 2. For the ranging data in Figs. 3 and 4, a slower slew rate of  $4 \text{ ns s}^{-1}$  was chosen to match the temporal duration of the overlap between the TPFC and signal comb with the inverse of the 26 -kHz measurement bandwidth.

Control loops in ranging system. For the dual-comb ranging demonstration of Figs. 3 and 4, the system operates as nested PLLs. The timing discriminator demodulation is implemented in an FPGA + DSP system with ±13 kHz of bandwidth centred around a demodulation frequency. The 26-kHz bandwidth in the demodulation limits the overall tracking bandwidth, but was chosen to demonstrate the high sensitivity by allowing for coherent integration over about (26 kHz)<sup>-1</sup> = 38 us to detect weak return signals. A broader bandwidth would sacrifice some sensitivity but allow for even faster tracking bandwidths. The output of the timing discriminator provides both a time and phase error signal. The time error signal is sent to a PII implemented on the DSP. This PII generates control trajectories for the tracking comb, which are sent via serial port to that comb's controller FPGA that runs the two PLLs for  $\theta_0(t)$  and  $\theta_N(t)$ at 50-kHz closed-loop bandwidth. The phase error could be similarly fed back directly to these PLLs controlling the TPFC. However, it is simpler, and equivalent, to instead direct the phase error to a PII implemented on the DSP, whose output is fed back to the direct digital synthesizer used to demodulate the approximately 10-MHz timing discriminator signals. The resulting frequency adjustment is time-stamped against the FPGA clock, which allows the accurate unwrapping of the carrier phase to determine the relative range change, as show in Fig. 4. With this choice of phase control, the tracking of the timing is implemented by changing only  $\theta_0(t)$  and leaving  $\theta_N(t)$  fixed, which avoids cross talk between the two loops.

#### Shot-noise limit for ranging

In Fig. 3c, we show our ranging measurements are shot-noise limited for received powers <10 nW by comparing measured range deviation to the expected shot-noise limited range deviation. Here we derive that theoretical shot-noise-limited range deviation.

We first assume the comb pulses have zero differential chirp and are Gaussian with an FWHM of  $\tau_{\rm p}$  in intensity. (The comb pulses pass through a Gaussian spectral filter before ranging). Their crosscorrelation then generates a Gaussian envelope. V, with a FWHM of  $2\tau_{\rm p}$ (because there is a factor of  $\sqrt{2}$  from the cross-correlation and the *E*-fields are also  $\sqrt{2}$  broader than the intensity of the comb pulses<sup>37</sup>). The detected heterodyne voltage signal has a carrier frequency set by the offset between the comb frequencies, but this carrier is removed in the demodulation to generate just the envelope signal. We assume the lock point is chosen at approximately the half-width at half-maximum point on this envelope. (The actual maximum slope is  $1\sigma$  from the peak, but this is a minor 6% correction at the cost of a reduced capture range). In that case, the change in voltage for small changes in the arrival time of the signal pulse with respect to the tracking (local oscillator) comb,  $\delta X$ , will be determined by the slope at the half-width at half-maximum point, or

$$\frac{\delta V}{\delta X} = \ln(2) \frac{V_{\text{peak}}}{\tau_{\text{p}}} [V \text{ s}^{-1}]$$
 (9)

where  $V_{\rm peak}$  is the maximum voltage measured when the signal and tracking comb pulses perfectly overlap. The inverse of this slope maps changes in V to changes in X. Voltage fluctuations from shot noise with a root-mean squared (r.m.s.) value of  $V_{\rm shotnoise}$  will show up as white timing jitter with an r.m.s. value of

$$\sigma_{\rm t} = \frac{\delta X}{\delta V} V_{\rm shotnoise}.$$
 (10)

In the strong local oscillator case (strong tracking comb pulses), the shot noise for the demodulated output is

$$V_{\text{shotnoise}} = eG \sqrt{\frac{2P_{\text{LO}}\eta B}{h\nu}}$$
 (11)

where e is the elementary charge constant, G is the transimpedance gain,  $P_{1:0}$  is the local oscillator power, h is Planck's constant, v is the carrier frequency,  $\eta$  is the quantum efficiency and B is the single-sided bandwidth with a corresponding averaging time  $T = (2B)^{-1}$  (ref. <sup>57</sup>). The peak signal,  $V_{\text{peak}}$ , is

$$V_{\text{peak}} = 2e\eta G \sqrt{\frac{P_{\text{LO}} P_{\text{s}}}{(\hbar \nu)^2}}$$
 (12)

where  $P_s$  is the total received signal-comb power on the detector<sup>57</sup>. Substitution of equations (10) and (11) into equation (9) using  $\tau = (2B)^{-1}$  and defining the total number of integrated signal photons in each measurement as  $n_s = P_s T/hv$  gives

$$\sigma_{\rm t} = \frac{1}{2\ln(2)} \frac{\tau_{\rm p}}{\sqrt{\eta n_{\rm s}}}.$$
 (13)

Then, converting to range, the shot-noise contribution to the range deviation is

$$\sigma_{\rm R} = \left(\frac{c}{2}\right) \frac{1}{\ln(2)} \frac{\tau_{\rm p}}{2\sqrt{\eta n_{\rm s}}}.$$
 (14)

In the actual implementation, a single heterodyne signal is insufficient as we need two measurements to normalize out the fluctuations in the received signal power (and therefore in  $V_{\rm peak}$ ). Therefore, the timing discriminator generates two time-displaced copies of the tracking comb pulses to generate the two displaced discriminator signals  $V_1$  and  $V_2$ , each of which has the same Gaussian shape and noise jitter as given above although with half the total power. The timing discriminator signal is given by the linear combination,  $S = (V_1 - V_2)/(V_1 + V_2)$ . An identical analysis for the shot-noise limited timing jitter and ranging jitter yields exactly the same equations (12) and (13), where  $n_s$  is the total number of signal photons.

The quantity in equation (13) is plotted in Fig. 3c as a function of  $P_s$  at a set averaging time of T=200 ms for the quantum efficiency  $\eta\approx 0.79$  and  $\tau_p=355$  fs, which is the time-bandwidth-limited pulse duration for the measured comb-pulse spectral FWHM of 10.1 nm.

The above derivation assumed the optimal situation that the two comb pulses have no differential chirp, are Gaussian, have unity mixing efficiency and the additive detector noise is zero. In equation (1), we include the numerical factor C to account for these and any other effects that increase the noise above this quantum-limited floor. In our case, the FWHM of the timing discriminator signals for pulses with zero differential chirp should be  $2\tau_p = 709$  fs, based on the measured spectral widths of the comb pulses, but we measure 824 fs for the data in Fig. 3c, indicating a differential dispersion between the pulses and corresponding timing jitter penalty of  $(824/709)^2 = 1.35$  (assuming the broadening both reduces the slope and the peak height, preserving the area). In addition, there is an SNR degradation of a factor of 1.39 owing to detector noise, measured non-idealities in interferogram slopes and spectral overlap. Finally, we measure an additional additive noise penalty of 1.065 in the radiofrequency chain. Combined, these imperfections give an expected value of  $C = (1.35) \times (1.39) \times (1.065) = 2.0$ , to be compared with the value of C = 2.16 measured from the upward displacement of the data points compared with the theoretical curve in Fig. 3c. These two values agree to within 8%. For the data in Fig. 4, the additional round-trip length of fibre optics in the path to the rail-mounted retroreflector added chirp to the signal comb that led to an additional 1.49-times penalty.

For the conventional dual-comb ranging using linear optical sampling, a similar analysis has been provided in Appendix B of ref. <sup>37</sup>. The performance curves in Fig. 5 are based on these equations and assume no additional penalties.

#### **Reporting summary**

Further information on research design is available in the Nature Research Reporting Summary linked to this article.

#### **Data availability**

The data for the figures in this paper are available for download at https://data.nist.gov/od/id/mds2-2703.

#### **Code availability**

The mathematics and algorithms necessary to create a time-programmable frequency comb are described between the main text and Methods.

- Sinclair, L. C. et al. Invited Article: A compact optically coherent fiber frequency comb. Rev. Sci. Instrum. 86, 081301 (2015).
- 57. Kingston, R. H. Detection of Optical and Infrared Radiation (Springer, 1978).

**Acknowledgements** We acknowledge J. Ellis, T. Fortier, K. Cossel, W. Swann, B. Stuhl and B. Washburn for discussions. We acknowledge funding from the National Institute of Standards and Technology.

**Author contributions** E.D.C., L.C.S., N.R.N. and J.-D.D. all contributed to the initial conception, the experiment design, the data acquisition, the analysis of the results and the writing of the manuscript.

 $\textbf{Competing interests} \ \text{The authors declare no competing interests}.$ 

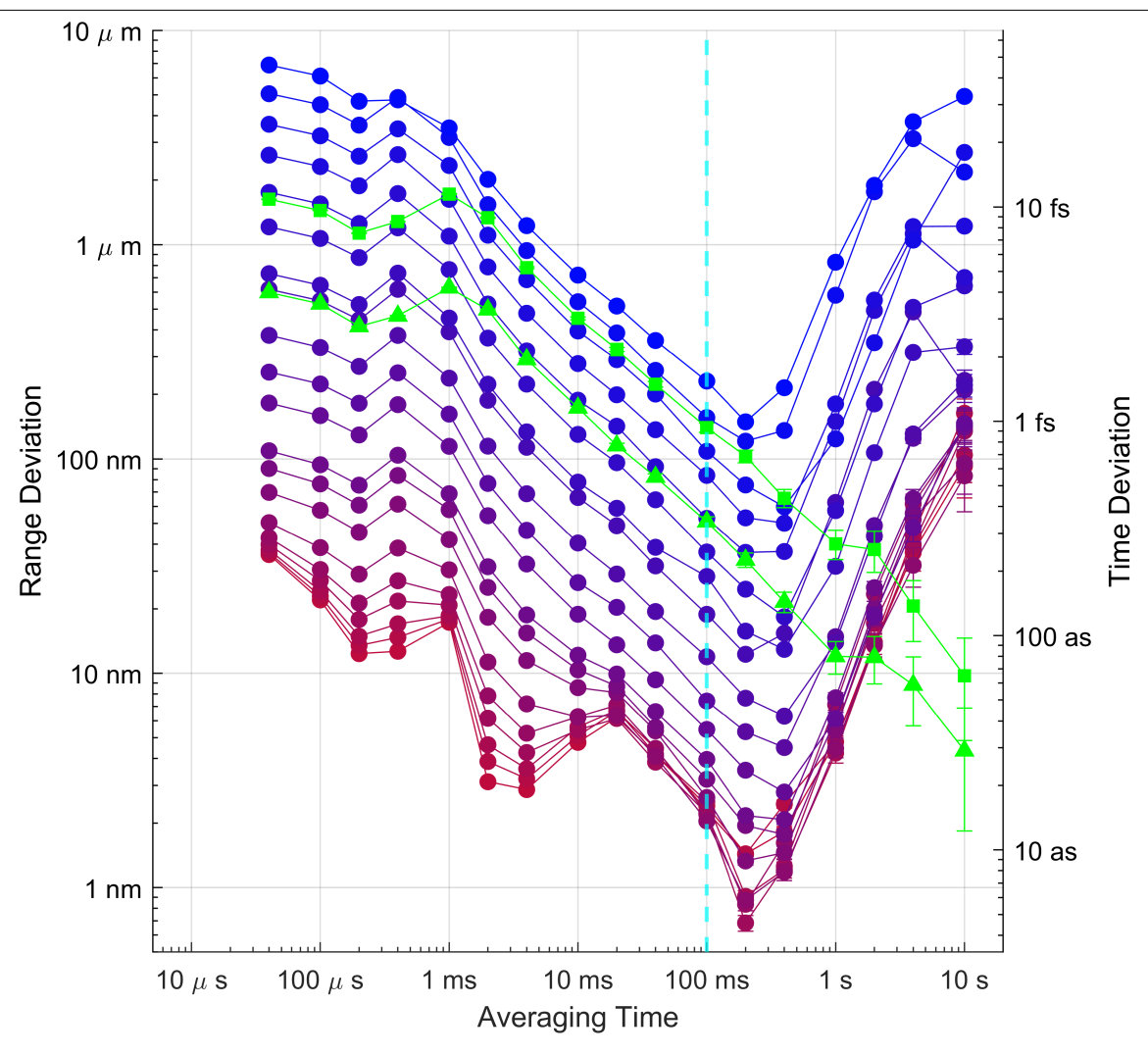
#### Additional information

**Supplementary information** The online version contains supplementary material available at https://doi.org/10.1038/s41586-022-05225-8.

**Correspondence and requests for materials** should be addressed to Laura C. Sinclair or Nathan R. Newbury.

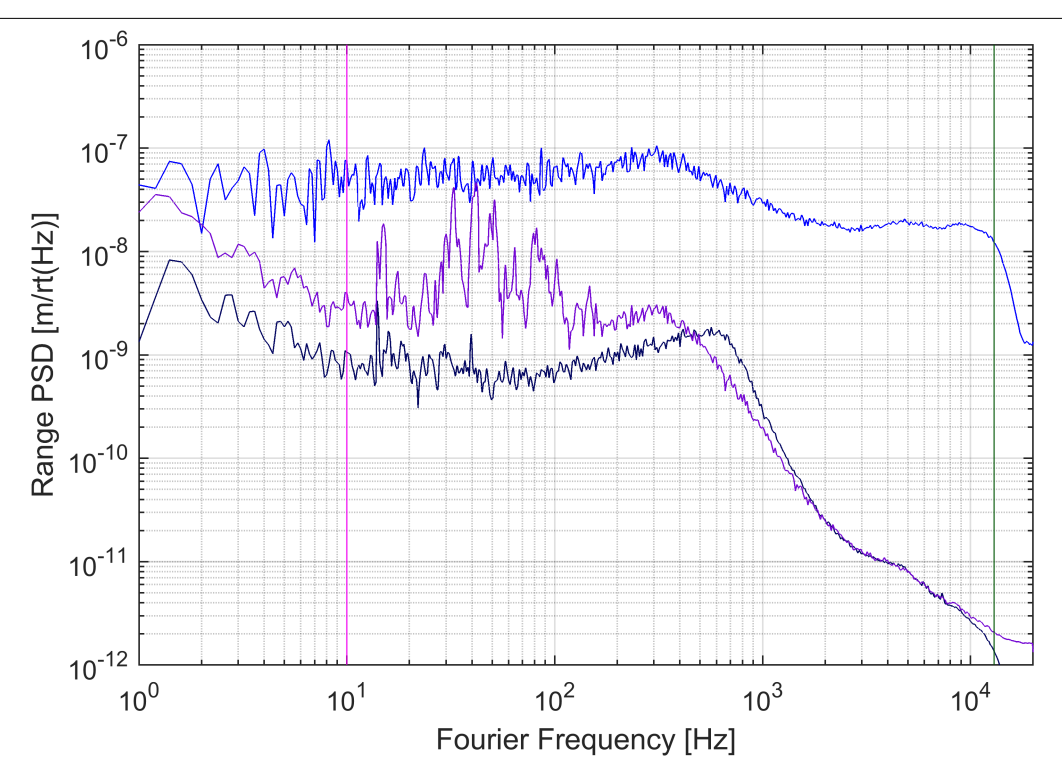
**Peer review information** *Nature* thanks Takuro Ideguchi, Xiaoxiao Xue and the other, anonymous, reviewer(s) for their contribution to the peer review of this work. Peer reviewer reports are available.

**Reprints and permissions information** is available at http://www.nature.com/reprints.



**Extended Data Fig. 1** | **Range deviation power comparison.** Range deviation (left axis) and time deviation (right axis) of dual-comb range measurements from a fixed reflection for signal-comb powers from 980 nW (bottom curve) down to 0.33 pW (top curve) with the following power levels  $\pm 10\%$ : 980 nW, 190 nW, 86 nW, 38 nW, 21 nW, 9.6 nW, 1.8 nW, 1.2 nW, 390 pW, 200 pW, 89 pW, 33 pW, 23 pW, 8.5 pW, 4.1 pW, 1.9 pW, 990 fW, 550 fW and 330 fW. The vertical dashed cyan line indicates the 200-ms averaging time for the data in Fig. 3c. Beyond 200-ms, the range deviation increases due to temperature-induced fluctuations in the fibre path up to the fixed reflection. In addition, the

deviations for the difference between the absolute range from the tracking comb timing and the relative range from the unwrapped carrier phase shift, from Fig. 4, are shown for the time periods of 60 to 100 seconds at 3.2 pW (green squares) and 110 seconds to 150 seconds at 32 pW (green triangles). For these data, the differential chirp between the signal and TPFC pulses was larger, leading to an additional 1.5x penalty in  ${\it C}$  and thus lie slightly above the curves at the same power for ranging off the fixed reflection (solid circles). However, because the path-length variation is common mode, the difference continues to average down beyond 200 ms.



**Extended Data Fig. 2** | **Range power spectral density.** Range power spectral density (PSD) for the data from Fig. 4 over the period of 60 s to 100 s at 3.2 pW return power for X(t) from the tracking comb (blue trace) and the unwrapped carrier phase  $\theta(t)$  (purple trace). Also shown is the noise floor for the unwrapped carrier phase (dark blue trace). The vibrations of the nominally immobile retroreflector can be clearly seen in the carrier-phase data. At the low

average power of 3.2 pW, the tracking dual-comb range shot-noise limited noise floor lies just above the minimal vibrations seen here. The vertical magenta line indicates the maximum 10 Hz update rate of FMCW while the vertical dark green line indicates the 13 kHz cut-off imposed by the 26 kHz measurement rate for the range data.

#### Extended Data Table 1 | Ranging modality comparison

Technique		olution, \( \lambda R \)	Non-Ambiguity Range, $R_{\it NA}$		Power penalty, $P_{\scriptscriptstyle P}$		Max. Update Rate, T-1	
FMCW Ranging <sup>a</sup> System 1 <sup>b,c</sup> B = 5 THz  (40 nm at 1550 nm)  C = 5 THz/s (40 nm/s)  System 2 <sup>b,d</sup>	$\frac{c}{2B}$	30 μm	$\sim \frac{cC}{4B}$	>> l <sub>coh</sub>	~1	0 dB	$\frac{C}{B}$	1 Hz
B= 1.3 THz (10 nm 1535 nm) C=12.5THz/s (100 nm/s)		115 μm						9.6 Hz
Conventional Dual- Comb Ranging								
Microcomb <sup>e</sup> : $B = \sim 2.5 \text{ THz}$ $f_{rep} = 100 \text{ GHz}$ $\Delta f_{rep} = 100 \text{ MHz}$		60 μm		0.15 cm		14 dB		~1 GHz
Er:fiber comb <sup>f</sup> : B = 1.2  THz (10 nm at 1560 nm) $f_{rep} = 200 \text{ MHz}$ $\Delta f_{rep} = 2 \text{ kHz}$	$\frac{c}{2B}$	125 μm	$\frac{c}{2f_{rep}}$	75 cm	$\sim rac{f_{rep}}{B}$	38 dB	$\frac{f_{rep}^2}{4B}$ For margin,	8.3 kHz
Ti:Sapph comb <sup>g</sup> : B = 0.3  THz (0.6 nm at 785 nm) $f_{rep} = 513 \text{ MHz}$ $\Delta f_{rep} = 130 \text{ kHz}$		510 μm		29 cm		27 dB	in practice this is often h $\frac{f_r^2}{16B}$	220 kHz
Dual-Comb Ranging with the TPFC B = 1.2  THz (10 nm at 1560 nm) Acquisition scans over	<u>c</u>	_	$rac{c}{2f_{rep}}$	75 cm	Acquisition: $\Delta XB$	0 to 30 dB	Acquisition: $S\Delta X$	40 Hz
$0 < \Delta X < f_{rep}^{-1}$ Update rate assumes $\Delta X = 1 \text{ ns (15 cm)}$ and $\Delta \dot{X} = 40 \text{ n/s}$	<u>2B</u>				Tracking: 1	0 dB	Tracking: $\frac{f_{rep}}{4}$	50 MHz

Comparison of parameters for FCMW ranging, conventional dual-comb ranging and the current TPFC-based dual-comb ranging. Scaling relationships and values from the literature are used to illustrate the trade-offs. All systems have a maximum range set by the laser coherence length. These values related to range, power penalty and maximum update rate were used to construct Fig. 5 of the main text. B: 3-dB bandwidth, C: chirp rate, C: speed of light (for simplicity ignoring the group index of air),  $I_{coh}$ : laser coherence length,  $I_{rep}$ : repetition frequency of comb,  $I_{rep}$ : offset in comb repetition frequencies,  $I_{rep}$ : pulse scan rate.

a Scaling for FMCW based on Barber, Z. W., Babbitt, Wm. R., Kaylor, B., Reibel, R. R. & Roos,. Appl Opt 49, 213–219 (2010).

<sup>&</sup>lt;sup>b</sup> The use of trade names in this manuscript is necessary to specify experimental results and does not imply endorsement by the National Institute of Standards and Technology.

 $<sup>^\</sup>circ \, System \, 1 \, specifications \, from \, Bridger \, Photonics \, data sheets \, (https://www.bridgerphotonics.com/).$ 

<sup>&</sup>lt;sup>d</sup> System 2 specifications from Luna Optical Backscatter Reflectometer (OBR) 4600 datasheet (https://lunainc.com).

Values taken from Trocha, P. et al. Science 359, 887–891 (2018). FWHM bandwidth estimated to be at 2.5THz from the manuscript figures.

 $<sup>^{\</sup>mathrm{f}}$  Values taken from Er:fibre comb system used also for the dual-comb system presented here.

<sup>&</sup>lt;sup>9</sup> Values taken from Mitchell, T., Sun, J., Sun, J. & Reid, D. T. Opt. Express 29, 42119-42126 (2021).

h This expression often appears with only a factor of two in the denominator. However, if the widths are all FWHM and assuming a filter that is not infinitely sharp, there would be significant aliasing in the signal if operated under these conditions leading to systematic range errors. We have used a factor of "4", which is still overly optimistic and the factor of "16" in the denominator is a more practical choice.

# nature portfolio

Corresponding author(s):	Laura Sinclair and Nathan Newbury
Last updated by author(s):	Jun 21, 2022

# **Reporting Summary**

Nature Portfolio wishes to improve the reproducibility of the work that we publish. This form provides structure for consistency and transparency in reporting. For further information on Nature Portfolio policies, see our <u>Editorial Policies</u> and the <u>Editorial Policy Checklist</u>.

Statistics				
For all statistical an	alyses, confirm that the following items are present in the figure legend, table legend, main text, or Methods section.			
n/a Confirmed				
The exact	act sample size (n) for each experimental group/condition, given as a discrete number and unit of measurement			
A stateme	tement on whether measurements were taken from distinct samples or whether the same sample was measured repeatedly			
<b>Y</b>	The statistical test(s) used AND whether they are one- or two-sided  Only common tests should be described solely by name; describe more complex techniques in the Methods section.			
A descript	A description of all covariates tested			
A descript	A description of any assumptions or corrections, such as tests of normality and adjustment for multiple comparisons			
	A full description of the statistical parameters including central tendency (e.g. means) or other basic estimates (e.g. regression coefficient AND variation (e.g. standard deviation) or associated estimates of uncertainty (e.g. confidence intervals)			
	For null hypothesis testing, the test statistic (e.g. <i>F</i> , <i>t</i> , <i>r</i> ) with confidence intervals, effect sizes, degrees of freedom and <i>P</i> value noted <i>Give P values as exact values whenever suitable.</i>			
For Bayesi	For Bayesian analysis, information on the choice of priors and Markov chain Monte Carlo settings			
For hierarchical and complex designs, identification of the appropriate level for tests and full reporting of outcomes				
Estimates	Estimates of effect sizes (e.g. Cohen's d, Pearson's r), indicating how they were calculated			
•	Our web collection on <u>statistics for biologists</u> contains articles on many of the points above.			
Software and	d code			
Policy information a	about <u>availability of computer code</u>			
Data collection	The mathematics and algorithms necessary to create a time programmable frequency comb are described between the main text and the methods section.			
Data analysis	The mathematics and algorithms necessary to create a time programmable frequency comb are described between the main text and the methods section.			

# Data

Policy information about availability of data

All manuscripts must include a data availability statement. This statement should provide the following information, where applicable:

For manuscripts utilizing custom algorithms or software that are central to the research but not yet described in published literature, software must be made available to editors and reviewers. We strongly encourage code deposition in a community repository (e.g. GitHub). See the Nature Portfolio guidelines for submitting code & software for further information.

- Accession codes, unique identifiers, or web links for publicly available datasets
- A description of any restrictions on data availability
- For clinical datasets or third party data, please ensure that the statement adheres to our policy

The data for the figures in this manuscript are available for download at https://data.nist.gov/sdp/<to be provided>/.

## Human research participants

Policy information about studies involving human research participants and Sex and Gender in Research.

Reporting on sex and gender

Use the terms sex (biological attribute) and gender (shaped by social and cultural circumstances) carefully in order to avoid confusing both terms. Indicate if findings apply to only one sex or gender; describe whether sex and gender were considered in study design whether sex and/or gender was determined based on self-reporting or assigned and methods used. Provide in the source data disaggregated sex and gender data where this information has been collected, and consent has been obtained for sharing of individual-level data; provide overall numbers in this Reporting Summary. Please state if this information has not been collected. Report sex- and gender-based analyses where performed, justify reasons for lack of sex- and gender-based analysis.

Population characteristics

Describe the covariate-relevant population characteristics of the human research participants (e.g. age, genotypic information, past and current diagnosis and treatment categories). If you filled out the behavioural & social sciences study design questions and have nothing to add here, write "See above."

Recruitment

Describe how participants were recruited. Outline any potential self-selection bias or other biases that may be present and how these are likely to impact results.

Ethics oversight

Identify the organization(s) that approved the study protocol.

Note that full information on the approval of the study protocol must also be provided in the manuscript.

# Field-specific reporting

Please select the one below that is the best fit for your research. If you are not sure, read the appropriate sections before making your selection.					
Life sciences	Behavioural & social sciences	Ecological, evolutionary & environmental sciences			

For a reference copy of the document with all sections, see <u>nature.com/documents/nr-reporting-summary-flat.pdf</u>

# Life sciences study design

All studies must disclose on these points even when the disclosure is negative.

Sample size

Describe how sample size was determined, detailing any statistical methods used to predetermine sample size OR if no sample-size calculation was performed, describe how sample sizes were chosen and provide a rationale for why these sample sizes are sufficient.

Data exclusions

Describe any data exclusions. If no data were excluded from the analyses, state so OR if data were excluded, describe the exclusions and the rationale behind them, indicating whether exclusion criteria were pre-established.

Replication

Describe the measures taken to verify the reproducibility of the experimental findings. If all attempts at replication were successful, confirm this OR if there are any findings that were not replicated or cannot be reproduced, note this and describe why.

Randomization

Describe how samples/organisms/participants were allocated into experimental groups. If allocation was not random, describe how covariates were controlled OR if this is not relevant to your study, explain why.

Blinding

Describe whether the investigators were blinded to group allocation during data collection and/or analysis. If blinding was not possible, describe why OR explain why blinding was not relevant to your study.

# Behavioural & social sciences study design

All studies must disclose on these points even when the disclosure is negative.

Study description

Briefly describe the study type including whether data are quantitative, qualitative, or mixed-methods (e.g. qualitative cross-sectional, quantitative experimental, mixed-methods case study).

Research sample

State the research sample (e.g. Harvard university undergraduates, villagers in rural India) and provide relevant demographic information (e.g. age, sex) and indicate whether the sample is representative. Provide a rationale for the study sample chosen. For studies involving existing datasets, please describe the dataset and source.

Sampling strategy

Describe the sampling procedure (e.g. random, snowball, stratified, convenience). Describe the statistical methods that were used to predetermine sample size OR if no sample-size calculation was performed, describe how sample sizes were chosen and provide a rationale for why these sample sizes are sufficient. For qualitative data, please indicate whether data saturation was considered, and what criteria were used to decide that no further sampling was needed.

Data collection

Provide details about the data collection procedure, including the instruments or devices used to record the data (e.g. pen and paper, computer, eye tracker, video or audio equipment) whether anyone was present besides the participant(s) and the researcher, and whether the researcher was blind to experimental condition and/or the study hypothesis during data collection.

Timing

Indicate the start and stop dates of data collection. If there is a gap between collection periods, state the dates for each sample cohort.

Data exclusions

If no data were excluded from the analyses, state so OR if data were excluded, provide the exact number of exclusions and the rationale behind them, indicating whether exclusion criteria were pre-established.

State how many participants dropped out/declined participation and the reason(s) given OR provide response rate OR state that no

Randomization

If participants were not allocated into experimental groups, state so OR describe how participants were allocated to groups, and if allocation was not random, describe how covariates were controlled.

# Ecological, evolutionary & environmental sciences study design

All studies must disclose on these points even when the disclosure is negative.

Non-participation

Data exclusions

Reproducibility

Randomization

Access & import/export

Disturbance

Blinding

Study description

Briefly describe the study. For quantitative data include treatment factors and interactions, design structure (e.g. factorial, nested, hierarchical), nature and number of experimental units and replicates.

Research sample

Describe the research sample (e.g. a group of tagged Passer domesticus, all Stenocereus thurberi within Organ Pipe Cactus National Monument), and provide a rationale for the sample choice. When relevant, describe the organism taxa, source, sex, age range and any manipulations. State what population the sample is meant to represent when applicable. For studies involving existing datasets, describe the data and its source.

Sampling strategy

Note the sampling procedure. Describe the statistical methods that were used to predetermine sample size OR if no sample-size calculation was performed, describe how sample sizes were chosen and provide a rationale for why these sample sizes are sufficient.

participants dropped out/declined participation.

Timing and spatial scale Indicate the start and stop dates of data collection, noting the frequency and periodicity of sampling and providing a rationale for these choices. If there is a gap between collection periods, state the dates for each sample cohort. Specify the spatial scale from which the data are taken

If no data were excluded from the analyses, state so OR if data were excluded, describe the exclusions and the rationale behind them, indicating whether exclusion criteria were pre-established.

Describe the measures taken to verify the reproducibility of experimental findings. For each experiment, note whether any attempts to repeat the experiment failed OR state that all attempts to repeat the experiment were successful.

Describe how samples/organisms/participants were allocated into groups. If allocation was not random, describe how covariates were controlled. If this is not relevant to your study, explain why.

Describe the extent of blinding used during data acquisition and analysis. If blinding was not possible, describe why OR explain why blinding was not relevant to your study.

Did the study involve field work? Yes No

# Field work, collection and transport

Field conditions Describe the study conditions for field work, providing relevant parameters (e.g. temperature, rainfall).

Location State the location of the sampling or experiment, providing relevant parameters (e.g. latitude and longitude, elevation, water depth).

Describe the efforts you have made to access habitats and to collect and import/export your samples in a responsible manner and in compliance with local, national and international laws, noting any permits that were obtained (give the name of the issuing authority, the date of issue, and any identifying information).

Describe any disturbance caused by the study and how it was minimized.

3

# Reporting for specific materials, systems and methods

We require information from authors about some types of materials, experimental systems and methods used in many studies. Here, indicate whether each material, system or method listed is relevant to your study. If you are not sure if a list item applies to your research, read the appropriate section before selecting a response.

Materials & experimental systems		Methods		
n/a	Involved in the study	n/a	Involved in the study	
$\boxtimes$	Antibodies	$\boxtimes$	ChIP-seq	
$\boxtimes$	Eukaryotic cell lines	$\boxtimes$	Flow cytometry	
$\boxtimes$	Palaeontology and archaeology	$\boxtimes$	MRI-based neuroimaging	
$\boxtimes$	Animals and other organisms			
$\boxtimes$	Clinical data			
$\boxtimes$	Dual use research of concern			